Supercell approach to the optical properties of porous silicon

M. Cruz

Escuela Superior de Ingeniería Mecánica y Eléctrica, UC, IPN, Mexico

M. R. Beltrán and C. Wang

Instituto de Investigaciones en Materiales, UNAM, Mexico Distrito Federal, 04510, Mexico

J. Tagüeña-Martínez and Yuri G. Rubo

Centro de Investigación en Energía, UNAM, Temixco, Morelos 62580, Mexico

We calculate the optical constants of porous silicon (por-Si) from the electronic band structure obtained by means of an sp^3s* tight-binding Hamiltonian and a supercell model, in which the pores are columns dug in crystalline Si. The position of the absorption edge of the material is defined by two competing effects: (i) transitions assisted by the scattering of carriers on the lattice of pores, which effectively decrease the ''indirectness'' of por-Si and result in a redshift of the absorption edge, and (ii) quantum confinement, which increases the band gap. The interplay between these effects is illustrated by calculating the imaginary part of the dielectric function for 8-, 32-, and 128-atom supercells with different porosities. We also show how the supercell model can be extended to take into account weak disorder, which produces nonvertical optical transitions in **k** space and smoothens the absorption spectra. Our results, obtained without any adjustable parameters, are compared with experimental data. [S0163-1829(99)05023-7]

I. INTRODUCTION

One of the dominant trends in current research in materials science and solid-state physics is the study of materials and devices at the nanometer scale. Porous silicon (por-Si), in particular, represents a very interesting nanostructured solid, rather than a simple collection of quantum dots or wires. This material has been extensively studied during the last eight years since the discovery of its efficient visible luminescence.[1] However, the effects of the pore morphology on the optical properties are not well understood.

Extensive experimental studies (for a recent comprehensive review see Ref. 2) have shown that the observed optical properties depend not only on the porosity but also on the way the por-Si sample is prepared. The preparation procedure modifies the morphology of por-Si, i.e., sizes, shapes, and interconnection of silicon quantum wires, which form por-Si. Therefore, it is important to have a model, beyond the effective mass approximation, which provides a better description of the energy-level structure of por-Si, and is able to incorporate the interconnectivity of the system. First-principles methods[3,4] are very successful in the calculation of the electronic structure of small Si nanocrystallites. Therefore, they give a good understanding of luminescence and recombination in por-Si, because it is now generally accepted that localized electron states are responsible for these phenomena.[5] However, cluster methods are not suitable for the analysis of extended states in the interconnected structure of por-Si, which could be very important for certain optical responses, such as absorption. This problem can be addressed within the framework of the supercell tight-binding model.[6] Semiempirical tight-binding calculations,[7–9] which use phenomenological parameters to include many-body effects not fully considered in a first-principles Hamiltonian,

are simple enough to be applied to large supercells with complex morphologies. It is known that the sp^3s* model overestimates the effective masses in the conduction band and, correspondingly, underestimates the opening of the band gap due to quantum confinement.[10] However, including d orbitals[11] or next-nearest-neighbor hopping[12] into this scheme not only leads to a substantial increase in computing time, but also does not necessarily improve the agreement with experimental data.[13]

In this paper we apply the semiempirical supercell approach[6] to calculate the interband optical transitions in por-Si. In this model, the pores are produced by removing columns of atoms within a supercell of crystalline Si (c-Si). Since the supercells are periodically repeated in the space, the resulting band structure can be described using the reduced Brillouin zone corresponding to the supercell, and all valence- and conduction-band states are characterized by the wave vector **k** belonging to this Brillouin zone. This zone is smaller in size than the c-Si one, and the band structures of c-Si and por-Si in the supercell model are substantially different. A peculiar feature of the band structure within this model for por-Si is the decrease in the difference between the direct and indirect gaps, both in energies and in their separation in the **k** space, which could be referred to as a decrease in the indirectness of the material. This tends to move the absorption edge to lower frequencies. On the other hand, the presence of pores produces partial quantum confinement of the carriers, which in turn leads to an increase of the band gap. This last effect depends substantially on the thickness of the silicon skeleton left between the pores, i.e., the spatial separation of the pores, and on their morphology. In particular, when the porosity is kept fixed, the value of the band gap increases with a decrease of the pore size and separation. We show in this paper that the onset of the absorption and the

frequency dependence of the absorption coefficient are defined by the interplay between these two competing effects. This is illustrated by the calculation of the imaginary part of the por-Si dielectric function $\varepsilon_2(\omega)$ in different supercells for a wide range of porosities. The results are compared also with available experimental data[14] for $\varepsilon_2(\omega)$.

Clearly, the supercell model does not contain any disorder, which is present in real por-Si samples, and in this idealized model for por-Si only vertical in **k**-space (momentum conserving) transitions are optically allowed. However, the pores in real samples are neither exactly parallel nor periodic columns, and moreover, there is an undulation of the silicon wires.[15] The existence of disorder is believed to be of key importance for the luminescence efficiency of por-Si, because it leads to the localization of electron-hole pairs, preventing their migration to nonradiative recombination centers.[16] The disorder affects the delocalized states as well, and the wave functions of carriers are not perfect Bloch functions. While the localization cannot easily be described within the supercell model, it is possible to incorporate some effects of disorder on the extended states, which are most relevant for the calculation of the absorption spectrum. Smooth and small disorder produces the dephasing of the electron wave function. When the typical length l on which the phase of the electron wave function becomes completely randomized due to the scattering (the dephasing length) is much greater than the wavelength of a carrier, $l \gg 2\pi/k$, one can allow for the disorder by replacing the δ function, which reflects momentum conservation in the transition-matrix element, by a weighting function with typical width l^{-1} in **k** space. This results in non-vertical interband transitions, giving a significant enlargement of the optically active **k** zone. The typical interval around each **k**-vector ("optical window"), where non-vertical transitions contribute, is about the inverse of the dephasing length. We present a discussion of this optical window and possible weighting functions. The optical window results mainly in overall smoothing of the absorption spectra. The dephasing of extended states in a random medium, responsible for the existence of an optical window, is a general effect. In particular, such dephasing is important for quantum phase transitions, like the superconductor-insulator transition produced by disorder.[17]

The paper is organized as follows. In Sec. II below we describe the supercell model and give the details of our evaluation of optical matrix elements with a comparative discussion of different approaches existing in the literature. Also, we present an extension of the supercell model to include small disorder. Section III contains the results of the calculations of the imaginary part of the dielectric function. Some of the results are compared with experimental data. Section IV is devoted to the conclusions. Finally, the Appendix considers the optical transitions in one undulating wire within the effective mass approximation to illustrate the existence of an optical window in **k** space.

II. THE SUPERCELL MODEL AND INTERBAND OPTICAL TRANSITIONS

In the supercell sp^3s^* tight-binding model, empty columns are produced by removing columns of Si atoms within the supercell along the [001] direction ($\hat{\mathbf{z}}$ axis). An 8-atom
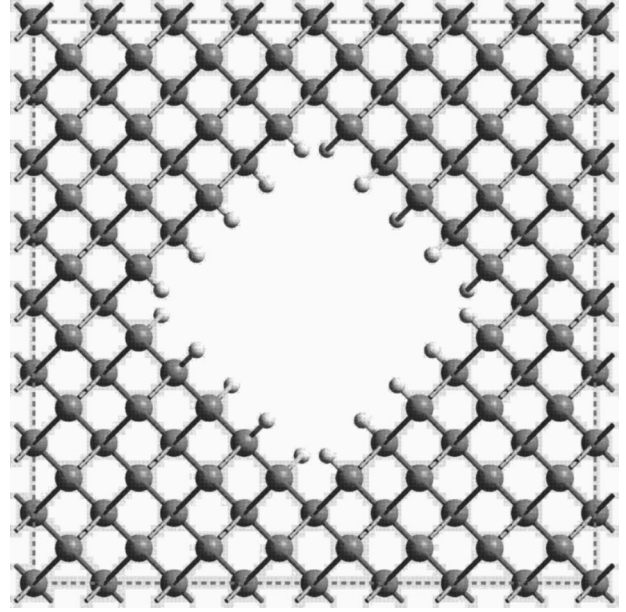

FIG. 1. Showing the 128-atom supercell with 25 Si atoms removed (19.53% porosity). The surface of the pore is saturated with hydrogen atoms, and por-Si is modeled by repeating this sort of supercell periodically.

supercell is a cube of side $a_0 = 5.431$ Å; a 32-atom supercell is built by joining four such cubes in the $X-Y$ plane, leading to a tetragonal structure with parameters $a_x = a_y \equiv a_t = 2a_0$ and $a_z \equiv a_l = a_0$. For a 128-atom supercell, the parameters are $a_t = 4a_0$ and $a_l = a_0$; an example of such supercell is shown in Fig. 1. Since por-Si exhibits a very large surface mainly hydrogen passivated, we saturate the pore surface with hydrogen atoms. In previous work[6] we have calculated the electronic band structure in a perfectly periodic porous structure, observing an enlargement and a tendency towards a direct energy band gap. To obtain optical constants from this model, it is necessary to evaluate also the dipole matrix elements (or oscillator strength), and within the tight-binding method there exist different approaches for these calculations.[18–21] We begin this section presenting the details of the approach we have used.

The optical properties of a material can be calculated from the oscillator strengths[22]

$$f_{v\mathbf{k},c\mathbf{k}'} = 2m \frac{|\langle c,\mathbf{k}'|\mathbf{e}\cdot\mathbf{v}|v,\mathbf{k}\rangle|^2}{E_c(\mathbf{k}') - E_v(\mathbf{k})},\qquad (1)$$

where $|v,\mathbf{k}\rangle$ and $|c,\mathbf{k}'\rangle$ are valence- and conduction-band eigenstates [with energies $E_v(\mathbf{k})$ and $E_c(\mathbf{k}')$, respectively], $\mathbf{v}$ is the electron velocity operator, and $\mathbf{e}$ is the polarization of light. In the tight-binding scheme the Bloch functions in Eq. (1) are linear combinations of atomic orbitals $|\mathbf{R}j\mu\rangle$, e.g.,

$$|v,\mathbf{k}\rangle = \frac{1}{\sqrt{N}} \sum_{\mathbf{R}j\mu} e^{i\mathbf{k}\cdot(\mathbf{R}+\mathbf{u}_j)} A_{j\mu}^v(\mathbf{k}) |\mathbf{R}j\mu\rangle,\qquad (2)$$

where **R** are the Bravais vectors giving the positions of supercells, j enumerates atoms within the supercell, μ identifies the orbital of the atom, $\mathbf{u}_j$ is the position of a given atom in supercell (so that $\mathbf{R}+\mathbf{u}_j$ is its actual position in the space),

and N is the number of supercells. In what follows, we will also use one combined index $\alpha \equiv \{j, \mu\}$, to avoid making some expressions too cumbersome.

The matrix elements of the electron velocity in Eq. (1) can be expressed, applying the definition $\mathbf{v} = (i/\hbar)[H, \mathbf{r}]$, via the matrix elements of the electron coordinate $\mathbf{r}$. In the spirit of the tight-binding model, the basic assumption is then to neglect the interatomic matrix elements of $\mathbf{r}$, since the overlapping of orbitals belonging to different atoms is supposed to be small. Namely,

$$(\mathbf{R}' \alpha' | \mathbf{r} | \mathbf{R}\alpha) \equiv (\mathbf{R}' j' \mu' | \mathbf{r} | \mathbf{R}j\mu)$$

$$= \{(\mathbf{R} + \mathbf{u}_j)\delta_{\mu\mu'} + \mathbf{d}_{\mu'\mu}\}\delta_{\mathbf{RR}'}\delta_{jj'}, \quad (3)$$

where the diagonal term is simply the position of the atom, and $\mathbf{d}_{\mu'\mu}$ is the intra-atomic dipole matrix element between different orbitals ($\mu \neq \mu'$). To transform the matrix element of velocity, we use the definition of the tight-binding Hamiltonian matrix in $\mathbf{k}$ space[23]

$$H_{\alpha'\alpha}(\mathbf{k}) = \sum_{\mathbf{R}} e^{-i\mathbf{k}\cdot(\mathbf{R}'+\mathbf{u}_{\alpha'})}(\mathbf{R}'\alpha'|H|\mathbf{R}\alpha)e^{i\mathbf{k}\cdot(\mathbf{R}+\mathbf{u}_\alpha)},$$

$$(4)$$

whose eigenfunctions are the expansion coefficients $A_\alpha^{c(v)}(\mathbf{k})$ for the Bloch functions, as in Eq. (2). Using Eqs. (4) and (3), we obtain

$$\langle c, \mathbf{k}' | \mathbf{e} \cdot \mathbf{v} | v, \mathbf{k} \rangle = \Phi(\mathbf{k}', \mathbf{k}) \frac{1}{N} \sum_{\mathbf{R}} e^{i(\mathbf{k}-\mathbf{k}')\cdot\mathbf{R}}, \quad (5)$$

$$\Phi(\mathbf{k}', \mathbf{k}) = \Phi_d(\mathbf{k}', \mathbf{k}) + \Phi_l(\mathbf{k}', \mathbf{k}), \quad (6)$$

where

$$\Phi_d(\mathbf{k}', \mathbf{k}) = \sum_{\alpha\alpha'} e^{i(\mathbf{k}-\mathbf{k}')\cdot\mathbf{u}_{\alpha'}} A_{\alpha'}^{c*}(\mathbf{k}') \left[\mathbf{e} \cdot \frac{dH_{\alpha'\alpha}(\mathbf{k})}{\hbar\, d\mathbf{k}} \right] A_\alpha^v(\mathbf{k}),$$

$$(7)$$

and

$$\Phi_l(\mathbf{k}', \mathbf{k}) = i\omega \sum_{j\mu\mu'} e^{i(\mathbf{k}-\mathbf{k}')\cdot\mathbf{u}_j} A_{j\mu'}^{c*}(\mathbf{k}')(\mathbf{e} \cdot \mathbf{d}_{\mu'\mu}) A_{j\mu}^v(\mathbf{k}).$$

$$(8)$$

In Eq. (8) ω stands for the transition frequency, $\omega = [E_c(\mathbf{k}') - E_v(\mathbf{k})]/\hbar$.

Functions $\Phi_d(\mathbf{k}, \mathbf{k}')$ and $\Phi_l(\mathbf{k}, \mathbf{k}')$ [Eq. (6)] originate, respectively from the first and the second term within the curly brackets of Eq. (3), and they describe physically different contributions to the velocity matrix element (5). $\Phi_d(\mathbf{k}, \mathbf{k}')$ exists as long as the Hamiltonian H has nonzero off-diagonal matrix elements between neighboring atoms, i.e., due to "hopping" of the electron from one atom to another, which produces the dispersion of the energy bands. This is why we refer to $\Phi_d(\mathbf{k}, \mathbf{k}')$ as the dispersion term. This contribution is specific to solids and can be expressed entirely through the Hamiltonian matrix, as is done in Eq. (7). In the perfect case, when the sum over $\mathbf{R}$ in Eq. (5) results in $\mathbf{k} = \mathbf{k}'$, it is just the off-diagonal element of the $\mathbf{k}$-space gradient of the tight-binding Hamiltonian matrix, which resembles the usual definition of velocity in free space. This way of calculating the oscillator strengths for the tight-binding scheme was suggested in Refs. 20 and 21 using different arguments. The second contribution $\Phi_l(\mathbf{k}, \mathbf{k}')$ [Eq. (8)] can be called the local term. This term cannot be expressed using the Hamiltonian matrix alone, since one needs additional information about the $\mathbf{r}$-space behavior of the atomic orbitals $|\mathbf{R}j\mu)$ to calculate the dipole matrix elements $\mathbf{d}_{\mu'\mu}$ in Eqs. (3) and (8). It is clear also if one considers the limiting case of no overlapping orbitals, when the energy bands are completely flat, so that all derivatives of $H_{\alpha'\alpha}(\mathbf{k})$ go to zero. In this case, however, the $\mathbf{d}_{\mu'\mu}$ are finite and $\Phi_l(\mathbf{k}, \mathbf{k}')$ describes the optical response of a collection of individual, independent atoms.

The dispersion and local terms, Eqs. (7) and (8), can be compared by estimating the value of $\Phi_l(\mathbf{k}, \mathbf{k}')$ as ωr_0, where r_0 is about the atomic radius. For most semiconductors the main contribution comes from the dispersion term $\Phi_l(\mathbf{k}, \mathbf{k}')$; for narrow-gap semiconductors, as InSb and $Hg_{1-x}Cd_xTe$, one has the strong inequality $\Phi_d(\mathbf{k}, \mathbf{k}') \gg \Phi_l(\mathbf{k}, \mathbf{k}')$. This implies that the polarizability of free atoms is much smaller than that of corresponding semiconductor.[24] The dispersion term only [in the $\mathbf{r}$-representation, i.e., as the first term in Eq. (3)], was taken into account in Ref. 19 when analyzing the optical properties of $Ga_{1-x}Al_xAs$ microclusters. It is not clear, however, whether this approximation is sufficient for the supercell por-Si model, especially for high porosities. First, this model exhibits substantial flattening of the energy bands, and second, it is believed that the relevance of the local term is increased when surface effects are considered.[25] We allowed for both terms in our calculations and used the parameters of Ref. 18 for $\mathbf{d}_{\mu\nu}$, obtained by fitting to the experimental data for $\varepsilon_2(\omega)$ in crystalline Si. For $\mathbf{e} \| \hat{\mathbf{x}}$, the values of the nonzero matrix elements are $(\mathbf{e} \cdot \mathbf{d}_{sp_x}) = 0.27$ Å and $(\mathbf{e} \cdot \mathbf{d}_{s*p_x}) = 1.08$ Å. It turns out that $\Phi_l(\mathbf{k}, \mathbf{k}')$ remains small with respect to $\Phi_d(\mathbf{k}, \mathbf{k}')$. Nevertheless, $\Phi_l(\mathbf{k}, \mathbf{k}')$ is important because the interference between local and dispersion terms makes a 25% contribution to the total absorption.

Using Eqs. (1) and (5) one can express the oscillator strength as

$$f_{v\mathbf{k},c\mathbf{k}'} = \frac{2m}{\hbar\omega}|\Phi(\mathbf{k}, \mathbf{k}')|^2 \frac{1}{N} \sum_{\mathbf{R}} e^{i(\mathbf{k}-\mathbf{k}')\cdot\mathbf{R}}. \quad (9)$$

By means of $f_{v\mathbf{k},c\mathbf{k}'}$ we calculate the imaginary part of the dielectric function $\epsilon_2(\omega)$ as[22]

$$\epsilon_2(\omega) = \frac{2\pi^2\hbar e^2}{m\omega V} \sum_{c,\mathbf{k}'} \sum_{v,\mathbf{k}} f_{v\mathbf{k},c\mathbf{k}'}\delta[E_c(\mathbf{k}') - E_v(\mathbf{k}) - \hbar\omega],$$

$$(10)$$

where $V \equiv Na^3$ is the normalization volume.

When the sum over $\mathbf{R}$ in Eq. (9) is expanded over all space, the oscillator strengths are nonzero only for $\mathbf{k} = \mathbf{k}'$, so that only "vertical" transitions in the $\mathbf{k}$ space of the reduced Brillouin zone are allowed. In reality, however, there is substantial disorder in the sizes and distribution of pores, and also there exist fluctuations in the diameter of the columns, which could be thought of as undulating rather than straight wires.[15] The simplest way to break the perfect periodicity and introduce disorder in the model under consideration could be to assume that the sum over $\mathbf{R}$ be restricted to a

finite volume with a typical length l. This value of l can be regarded as the typical dephasing length for the electron wave function. In this case, instead of $\delta(\mathbf{k}-\mathbf{k}')$ in Eq. (9) we have

$$\sum_{\mathbf{R}} e^{i\Delta\mathbf{k}\cdot\mathbf{R}} = \frac{\sin(\frac{1}{2}l_t\Delta k_x)\sin(\frac{1}{2}l_t\Delta k_y)\sin(\frac{1}{2}l_l\Delta k_z)}{\sin(\frac{1}{2}a_t\Delta k_x)\sin(\frac{1}{2}a_t\Delta k_y)\sin(\frac{1}{2}a_l\Delta k_z)},$$

(11)

where a_t and a_l are the supercell constants, and l_t and l_l are the transverse and longitudinal dephasing lengths, respectively. In this approximation not only vertical, but also non-vertical transitions within a window $\Delta k_i \sim l_i^{-1}$ around each $\mathbf{k}$ vector are allowed. These transitions are weighted with a function given by Eq. (11). The lengths l_i should obviously be much greater than the supercell constant, $l_i \gg a_i$, otherwise the use of $\mathbf{k}$ space for classifying the states would be not valid. The existence of an optical window is a consequence of the disorder in the system; we illustrate this statement in the Appendix, where we consider the dipole matrix element for one undulating quantum wire within the effective mass approximation. As shown in the Appendix, the shape of the weighting function depends on the type of disorder.

Before proceeding to the results of our calculations, we would like to make some qualitative remarks about the optical properties of the supercell model. As mentioned already, the por-Si structure is simulated in this model by a periodic repetition the space of a large Si supercell (which could contain up to 128-Si atoms), and the wave vectors $\mathbf{k}$ and $\mathbf{k}'$ in Eqs. (1),(10) belong to a reduced Brillouin zone. If we apply this model to crystalline Si, its electronic structure will then consist of sets of conduction and valence bands, which can be deduced by folding the usual Si bands into a reduced Brillouin zone. When a column of Si atoms is removed and dangling bonds are saturated with hydrogen, this supercell becomes the primitive cell for the material, and this affects the band gap of the material and the shape of the bands. The resulting band structure is shown in Fig. 2 for 8-, 32-, and 128-atom supercell. In all three cases the porosity is the same, 12.5%, which is achieved by removing 1, 4, and 16 Si atoms, respectively. It should be pointed out that although the porosity is the same, the morphology (sizes and spatial separation of pores) is different. A remarkable feature seen from Fig. 2 in all cases is a decrease of the energy difference ΔE_g between the direct and indirect band gaps, with respect to crystalline Si. For instance, for the 8-atom supercell [Fig. 2(a)] $\Delta E_g \approx 130$ meV. We will refer to this effect as the *decrease in the indirectness* of the material. The second feature, is the strong dependence of the gap on the thickness of the Si skeleton, i.e., the gap widens as the thickness gets thinner, which we will refer as *quantum quasiconfinement*. Note, however, that in spite of this widening of the gap, the electron states are delocalized in the supercell model. These two competing effects define the position of the absorption edge of por-Si. In particular, for the 128-atom supercell at small porosities, the band structure is very similar to that of folded c-Si one, but the optical absorption is expected to start at lower energies. This tail of the absorption spectrum can be thought of as originating from umklapp processes when op-
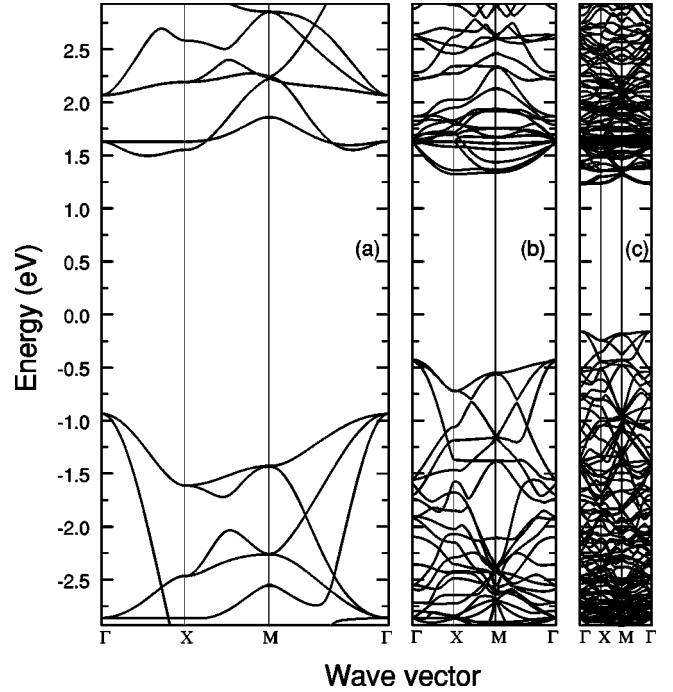

FIG. 2. Showing the band structure for por-Si of porosity 12.5%, using (a) an 8-atom supercell (with 1 atom removed), (b) a 32-atom supercell (with 4 atoms removed), and (c) a 128-atom supercell (with 16 atoms removed).

tical transitions in crystalline Si are accompanied by Bragg scattering on the superlattice of the introduced pores.

III. CALCULATIONS OF THE DIELECTRIC FUNCTION

The calculations have been carried out for light polarized in the [100] direction, i.e., perpendicular to the pore alignment. First, we present the dependence of the imaginary part of the dielectric function $\varepsilon_2(\omega)$ on the sample morphology, which was qualitatively discussed at the end of previous section. In order to avoid complications, we have studied only highly symmetric pores. In this case the same porosity of 12.5% can be achieved, as mentioned above, for all supercells under consideration, and the $\varepsilon_2(\omega)$ obtained are shown in Fig. 3. They have been calculated as described in Sec. II sampling the Brillouin zone by 1 685 159, 13 357, and 425 $\mathbf{k}$ points for 8-, 32-, and 128-atom supercells, respectively. The data correspond to the perfect case when no disorder is included, which results in only vertical interband transitions, i.e., $\mathbf{k}=\mathbf{k}'$. Making allowances for an optical window does not change these plots substantially. The onset of optical absorption corresponds to the value of their band gaps, as seen from comparison of Figs. 3 with 2, where the band structures for the same three cases is presented. The values of the direct band gap E_g are 2.54, 1.88, and 1.38 eV for 8-, 32-, and 128-atom supercells, respectively. This remarkable effect on the value of the gap is due to different quantum quasiconfinements, i.e., due to an increase in the difference between the pores and their diameters, as the supercell increases with a constant porosity. Note, that in the case of the 128-atom supercell the absorption is very weak for the photon energy range $1.38-2.50$ eV. This happens because of the small oscillator strengths in this region. The matrix ele-
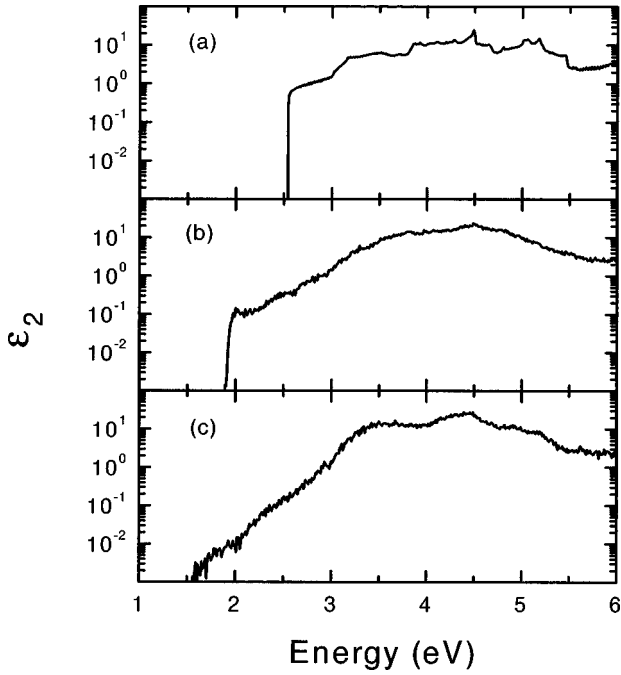
FIG. 3. Imaginary part of the dielectric function, $\varepsilon_2(\omega)$, versus the photon energy for the same cases as in Fig. 2. (a) An 8-atom supercell (with 1 atom removed), (b) a 32-atom supercell (with 4 atoms removed), and (c) a 128-atom supercell (with 16 atoms removed).

ment arises in second-order perturbation theory, and the transitions are in fact indirect optical processes in the c-Si matrix, assisted by the scattering on the pores.

To analyze the dependence of $\varepsilon_2(\omega)$ on the porosity, one has to perform calculations on big supercells, where the porosity can be changed progressively. Figure 4 presents such dependences obtained for the 128-atom supercell, with some central Si atoms removed to produce a symmetric pore. Higher porosities than 32.28% are not shown, since we have kept the orientation of the pores for all cases as in Fig. 1, which corresponds to a 19.53% porosity. For very small porosities it is interesting to compare our results with the crystalline Si case, shown in the same figure with the label 0% porosity. The remarkable feature seen from Fig. 4 is the appearance of a low-frequency tail in the function $\varepsilon_2(\omega)$ for porous Si. This tail is connected to a decrease of the indirectness of the material, which comes from the optical transition assisted by the scattering on the pores, as discussed above. With an increase of porosity, quantum confinement comes into play and produces the blueshift of this tail.

We have also performed our calculations for a porosity of 76.56% (98 atoms removed from a 128-atom supercell), which is the highest possible porosity with a square pore for this supercell. These results, calculated with 1225 **k** points in the reduced Brillouin zone, are compared with the experimental data of Ref. 14 in Fig. 5. For such high porosities the optical absorption in the perfect case consist of a set of peaks (thin-solid line in Fig. 5), which arise from very flat bands. Calculating $\varepsilon_2(\omega)$ for this case, we have taken also into account the effect of disorder and have introduced an optical window to include non-vertical transitions, as discussed in Sec. II. The resulting spectrum (thick-solid line) becomes smoother. The size of the optical window used in these cal-
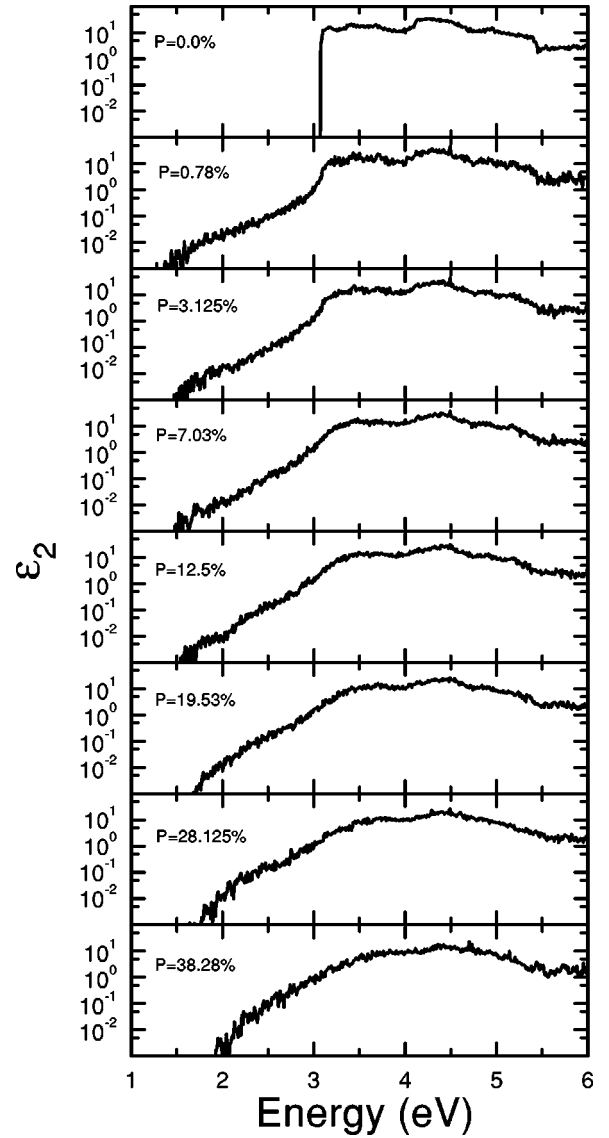

FIG. 4. Showing the low-frequency tail of the imaginary part of the dielectric function, $\varepsilon_2(\omega)$, as a function of photon energy for different porosities. The calculations were performed using 225 **k** points in the Brillouin zone.

culations corresponds to the dephasing lengths $l_l = l_t$ $= 108$ Å. Despite the fact that our theory gives, without any adjustable parameters, the value of the peak in good agreement with the experiment (dashed line), there is a discrepancy at the onset of absorption. The blueshift of the theoretical curve could be due to a slightly higher porosity in the calculations. Note that the experiments were performed at 70% porosity. However, we believe that the main difference in the position of the onset is due to different quantum quasiconfinements. To reproduce the data of Ref. 14 one needs to perform the calculations on a bigger supercell. Note also that the experiments were performed for at room temperature; the temperature additionally smoothens the optical response.

IV. CONCLUSIONS

The supercell model for por-Si presented above demonstrates the interplay between two main features of this mate-
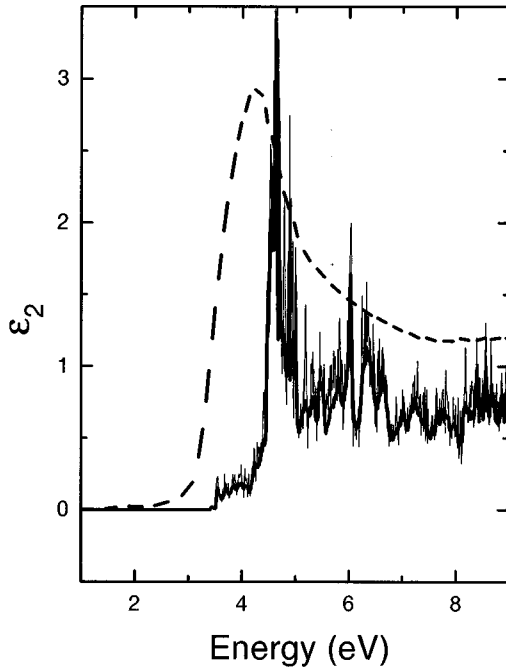
FIG. 5. Comparison of the experimental dielectric function for 70% porous Si (dashed line) with our calculations for the 128-atom supercell model at 76% porosity. The thin-solid line represents the response in the perfect case (vertical optical transitions), and the smoothening of the curve by disorder (vertical and nonvertical transitions) is given by the thick-solid line (see text). The experimental data are presented by digitizing the plot of Ref. 14.

rial: quantum quasiconfinement and the reduction of the gap for direct optical transitions. The competition between these two effects defines the position of the absorption edge and makes it possible to tune the onset of absorption in a wide energy range. By quantum quasiconfinement we mean the substantial enlargement of the gap with the decrease in the interpore distance, although electrons and holes are not localized within this model. The reduction of the gap comes from the decrease in indirectness of the material, which can be thought as due to the appearance of new absorption processes, when the transitions are assisted by scattering on the pores. The model could also take into account a small amount of disorder by allowing nonvertical **k**-space transitions. This results in the smoothing of the absorption spectrum in the high-porosity case. This simple microscopic quantum-mechanical tight-binding treatment is capable of reproducing the shape of the dielectric function of por-Si. The position of the absorption peak is very sensitive to the confinement of carriers in the por-Si sample, and can be used to extract information about the size of Si quantum wires. The supercell model can be further improved to include other saturators of the pore surface (e.g., oxygen), surface relaxation and amorphization. These studies are currently in progress.
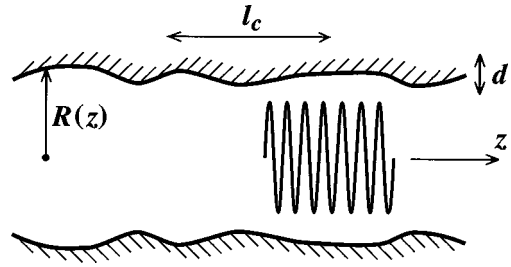
FIG. 6. The geometry of an undulating wire. The fluctuations of the radius of the wire are small compared to R_0 and they are smooth on the electron wavelength.

APPENDIX: UNDULATING WIRE

The goal of this appendix is to consider, within the effective mass approximation, the electron states and dipole matrix elements for the intersubband transitions in a quantum wire with fluctuating radius (undulating wire). The geometry of the wire is shown on Fig. 6. The radius of the wire exhibits random fluctuations as a function of the direction z along the wire, $R \equiv R(z) = R_0 + \delta R(z)$ with the average $\langle \delta R(z) \rangle = 0$. The fluctuations of the radius are supposed to be Gaussian and uniform along the wire, so that their statistics are completely defined by the correlator $\Phi(z - z') = \langle \delta R(z) \delta R(z') \rangle$. In what follows we will assume that the typical amplitude of fluctuation d is small, $d \equiv \Phi(0)^{1/2} \ll R_0$, and denote the correlation length of the random function $\delta R(z)$ [i.e., the typical length on which $\Phi(z)$ decays to zero] as l_c. One can define $l_c = (2d^2)^{-1} \int \Phi(z) dz$.

We shall consider here the optical transitions between the states with zero-angular momentum ($L_z = m = 0$), which are produced by the $\hat{\mathbf{z}}$-polarized light. In the absence of fluctuations, these states are classified by the wave vector k in the $\hat{\mathbf{z}}$ direction and the subband number $n = 1, 2, 3, \ldots$, and they have energies $E = \varepsilon_n(R_0) + \hbar^2 k^2 / 2m^*$. The corresponding unperturbed electron wave functions can be written in cylindrical coordinates as

$$\psi_{nk}^{(0)}(R_0; \rho, z) = L^{-1/2} \phi_n(R_0, \rho) \exp(ikz). \qquad \text{(A1)}$$

In this expression, $\phi_n(R_0, \rho)$ is proportional to the Bessel function $J_0[\kappa_n(R_0)\rho]$, where $\kappa_n(R_0) = \sqrt{2m^* \varepsilon_n(R_0)}/\hbar$, and L is a normalization length. For the case of a wire with infinite walls one has $\kappa_n(R_0) = c_n / R_0$, with the numbers c_n standing for the zeros of the Bessel function: $c_1 \approx 2.405$, $c_2 \approx 5.520$, etc.

To investigate the effect of undulation on electron wave functions and the dipole matrix elements one has to go beyond simple perturbation theory. This could be done for high velocities of electron when $k l_c \gg 1$, i.e., when the fluctuation of the radius of the wire are smooth on the electron wavelength (cf. with the last problem in §45 of Ref. 26). In this "adiabatic" case, the wave functions for the undulating wire $\psi_{nk}(\rho, z)$ can be found by neglecting the intersubband

mixing, i.e., $\psi_{nk}(\rho,z)=f(z)\psi_{nk}^{(0)}[R(z);\rho,z]$. Substituting this function into the Schrödinger equation one can neglect, for $kl_c\gg1$, the second derivative of $f(z)$, which is much smaller than the term with the first derivative (proportional to k). Then we have

$$-i(\hbar^2/m^*)kf'(z)+\delta\varepsilon_n(z)f(z)=0, \qquad (A2)$$

$$\psi_{nk}(\rho,z)=\exp\left[-\frac{im^*}{\hbar^2k}\int^z\delta\varepsilon(z')dz'\right]\psi_{nk}^{(0)}[R(z);\rho,z], \qquad (A3)$$

where $\delta\varepsilon(z)$ is the fluctuation of the subband energy,

$$\delta\varepsilon_n(z)=\varepsilon_n[R(z)]-\varepsilon_n(R_0)\approx-2\varepsilon_n(R_0)\frac{\delta R(z)}{R_0}. \quad (A4)$$

The wave functions (A3) can be used to calculate the dipole matrix element $M_{nn'}(k,k')$ for the optical transition $(n,k)\rightarrow(n',k')$. If we account for disorder the "nonvertical" transitions $(k'\neq k)$ are allowed; however $|k'-k|\ll|k|$ under the assumptions made. To find the shape of the weighting function for the nonvertical transitions one has to average $|M_{nn'}(k,k')|^2$, which is proportional to

$$\int dzdz'\,e^{i(k-k')(z-z')}\exp\left[-iQ_{nn'}^2\int_{z'}^z\delta R(\zeta)d\zeta\right], \qquad (A5)$$

over the random function $\delta R(\zeta)$. In Eq. (A5) we denoted

$$Q_{nn'}^2=\frac{2m^*\Delta\varepsilon_{nn'}^{(0)}}{\hbar^2kR_0}=\frac{c_{n'}^2-c_n^2}{kR_0^3}, \qquad (A6)$$

and $\Delta\varepsilon_{nn'}^{(0)}=\varepsilon_{n'}(R_0)-\varepsilon_n(R_0)$. Performing this averaging one finds that $\delta(k-k')$, present in $M_{nn'}(k,k')$ without disorder, should be replaced by

$$\int\frac{dz}{2\pi}e^{i(k-k')z}\exp\left[-Q_{nn'}^4\int_0^{|z|}(|z|-\zeta)\Phi(\zeta)d\zeta\right]. \qquad (A7)$$

It is seen from Eq. (A7) that the shape of the weighting function depends on the interrelation between the reciprocal correlation length l_c^{-1} and the characteristic wave vector $\varkappa=d^2l_cQ_{nn'}^4$. For $\varkappa l_c\ll1$ the integral in the exponent in Eq. (A7) should be calculated for large $|z|$, which leads to a Lorentzian with width $\varkappa$. In the opposite case, $\varkappa l_c\gg1$, the main contribution comes from $|z|\ll l_c$, and the line is Gaussian with the dispersion $dQ_{nn'}^2$. In the intermediate case, the result depends on a particular form of correlator $\Phi(\zeta)$ and should be found from Eq. (A7) numerically.

The broadening of the transition line considered in this Appendix can be referred as quasiclassical. The above derivation does not take into account the effects of quantum localization. These effects were considered for undulating Si wires in Refs. 27–29.

[1] L. T. Canham, Appl. Phys. Lett. **57**, 1046 (1990); A. G. Cullis and L. T. Canham, Nature (London) **353**, 335 (1991); L. T. Canham, M. R. Houlton, W. Y. Leong, C. Pickering, and J. M. Keen, J. Appl. Phys. **70**, 422 (1991).

[2] A. G. Cullis, L. T. Canham, and P. D. J. Calcott, J. Appl. Phys. **82**, 909 (1997).

[3] F. Buda, J. Kohanoff, and M. Parrinello, Phys. Rev. Lett. **69**, 1272 (1992).

[4] S. Öğüt, J. R. Chelikowsky, and S. G. Louie, Phys. Rev. Lett. **79**, 1770 (1997).

[5] P. D. J. Calcott, Mater. Sci. Eng., B **51**, 132 (1998).

[6] M. Cruz, C. Wang, M. R. Beltrán, and J. Tagüeña-Martínez, Phys. Rev. B **53**, 3827 (1996).

[7] G. D. Sanders and Y. C. Chang, Phys. Rev. B **45**, 9202 (1992).

[8] M. Lannoo, C. Delerue, and G. Allan, J. Lumin. **70**, 170 (1996).

[9] N. A. Hill and K. B. Whaley, Phys. Rev. Lett. **75**, 1130 (1995).

[10] C. Delerue, M. Lannoo, and G. Allan, Phys. Rev. Lett. **76**, 3038 (1996).

[11] J. M. Jancu, R. Scholz, F. Beltram, and F. Bassani, Phys. Rev. B **57**, 6493 (1998).

[12] J. P. Proot, C. Delerue, and G. Allan, Appl. Phys. Lett. **61**, 1948 (1992); C. Delerue, G. Allan, and M. Lannoo, Phys. Rev. B **48**, 11 024 (1993).

[13] N. A. Hill and K. B. Whaley, Phys. Rev. Lett. **76**, 3039 (1996).

[14] N. Koshida, H. Koyama, Y. Suda, Y. Yamamoto, M. Araki, T. Saito, and K. Sato, Appl. Phys. Lett. **63**, 2774 (1993).

[15] A. G. Cullis and L. T. Canham, Nature (London) **353**, 335 (1991).

[16] A. J. Read, R. J. Needs, K. J. Nash, L. T. Canham, P. D. J. Calcott, and A. Qteish, Phys. Rev. Lett. **69**, 1232 (1992).

[17] A. M. Goldman and N. Marković, Phys. Today **51** (11), 39 (1998), and references therein.

[18] A. Selloni, P. Marsella, and R. Del Sole, Phys. Rev. B **33**, 8885 (1986).

[19] B. Koiller, R. Osório, and L. M. Falicov, Phys. Rev. B **43**, 4170 (1991).

[20] L. C. Lew Yan Voon, and L. R. Ram-Mohan, Phys. Rev. B **47**, 15 500 (1993).

[21] M. Graf and P. Vogl, Phys. Rev. B **51**, 4940 (1995).

[22] W. A. Harrison, *Electronic Structure and the Properties of Solids* (Dover, New York, 1989), Chap. 4.

[23] P. Vogl, H. P. Hjalmarson, and J. D. Dow, J. Phys. Chem. Solids **44**, 365 (1983).

[24] L. Brey and C. Tejedor, Solid State Commun. **48**, 403 (1983).

[25] R. Del Sole (private communication).

[26] L. D. Landau and E. M. Lifshits, *Quantum Mechanics (Nonrelativistic Theory)* (Addison-Wesley, Reading, MA, 1965).

[27] N. A. Hill and K. B. Whaley, J. Electron. Mater. **25**, 269 (1996).

[28] F. Bentosela, P. Exner, and V. A. Zagrebnov, Phys. Rev. B **57**, 1382 (1998).

[29] I. G. Tigelis, J. P. Xanthakis, and J. L. Vomvoridis, Phys. Status Solidi B **165**, 125 (1998).